Pergamon

Tetrahedron 56 (2000) 1797–1810

TETRAHEDRON

Stereochemistry and Conformational Analysis of Hemirubin

Michael T. Huggins and David A. Lightner*

Department of Chemistry, University of Nevada, Reno, NV 89557, USA

Received 14 December 1999; revised 25 January 2000; accepted 27 January 2000

Abstract—Intramolecularly hydrogen-bonded analogs of the natural bile pigment, bilirubin, are very scarce. Nuclear Overhauser effect NMR studies of the newest analog, a hemirubin (**1**), confirms intramolecular hydrogen bonding and a ridge-tile-shaped conformation. ^{1}H NMR studies of **1** at sufficiently low temperatures detect conformational enantiomerization, for which an activation barrier of $\Delta G^{\ddagger}\sim$16 kcal/mol at 25°C in $CDCl_3$ has been estimated. Evidence for the presence of dimeric association at low temperatures or high concentrations of **1** is found by the appearance of new sets of resonances, data from which may be used to calculate: $\Delta G^{\circ}_{298\ K}$ +3.4 kcal/mol, ΔH° −5.6 kcal/mol and ΔS° −30.3 cal/deg/mol.

Introduction

Bilirubin (Fig. 1), the yellow–orange end-product of heme metabolism and the colorful herald of hepatobiliary disease,[1,2] consists of twin dipyrrinones conjoined to a $-CH_2-$ group. Dipyrrinones are bright yellow chromophores and avid participants in hydrogen bonding.[3,4] In bilirubin they may rotate independently about the $-CH_2-$, but only one conformation, shaped like a half-opened book, lies at a global energy minimum.[5,6] And this conformation (Fig. 1B) is further stabilized by intramolecular hydrogen bonds that link each dipyrrinone with an opposing propionic acid.[7,8] Taken collectively, the matrix of six intramolecular hydrogen bonds dominates the stereochemistry of bilirubin and profoundly controls its solution, spectroscopic and metabolic properties.

Various dipyrrinone models for bilirubin have been synthesized and found useful in understanding the spectroscopic properties and photochemical reactions of the natural pigment.[3,9,10] However, these analogs typically lacked the intramolecular hydrogen bonding so essential to bilirubin—until the very recent syntheses of two analogs with (i) three pyrrole rings (**3**)[11] and (ii) only two pyrrole rings (hemirubin, **2**).[12] Tripyrrole **3** was found to engage in intramolecular hydrogen bonding in the crystal and in solution in nonpolar solvents. Hemirubin **2** is believed to engage in intramolecular hydrogen bonding, but its solubility in nonpolar solvents such as $CDCl_3$ and CD_2Cl_2 was too limited to permit a detailed analyses of conformation by NMR techniques. To overcome this obstacle, we synthesized a new hemirubin (**1**) and its 10-oxo analog (**4**), both of which have excellent solubility in non-polar organic

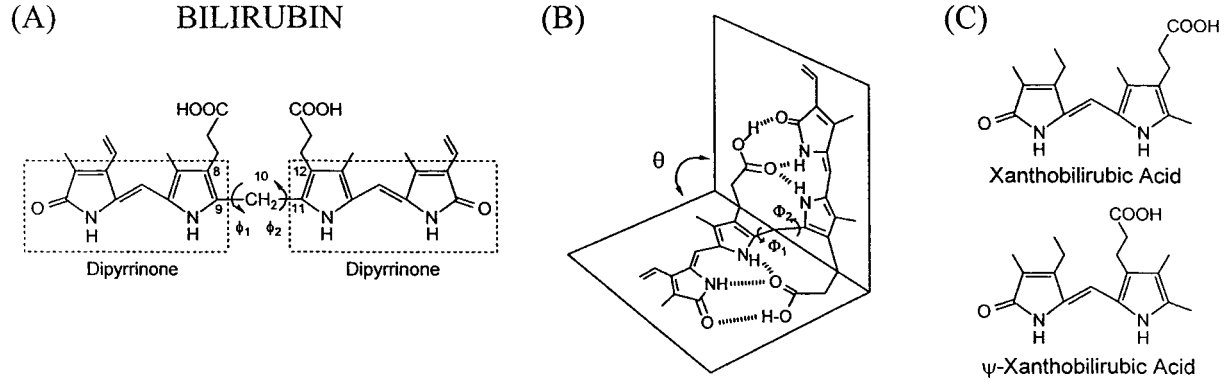

Figure 1. (A) Bilirubin in a high energy linear conformation with angles of rotation designated as ϕ_1 and ϕ_2 about the C(9)–C(10) and C(10)–C(11) bonds. (B) Preferred bilirubin conformation shaped like a ridge-tile ($\phi_1=\phi_2\sim60°$) with an interplanar angle $\theta\sim100°$. This conformation achieves considerable stabilization from intramolecular hydrogen bonds (hatched lines). (C) Dipyrrinone propionic acid analogs of bilirubin.

Keywords: pyrroles; hydrogen bonding; stereoisomerism.

* Corresponding author. Tel.: +1-775-784-4980; fax: +1-775-784-6804; e-mail: lightner@unr.edu

0040–4020/00/$ - see front matter
PII: S0040-4020(00)00087-9

solvents. In the following we describe (i) their syntheses, and (ii) their conformational analysis by molecular dynamics calculations and by systematic analyses of nuclear Overhauser effects (NOEs) and variable temperature ^{1}H NMR (VT-NMR) spectroscopic analysis. The study of **1** provides insights into how the conformation and solution properties of bilirubin are controlled by intramolecular hydrogen bonding. The 10-oxo-hemirubins, e.g. **4**, serve as models for 10-oxo-bilirubin, which is thought to be implicated in alternate (oxidative) pathways for bilirubin elimination and mammalian metabolism.[13,14]

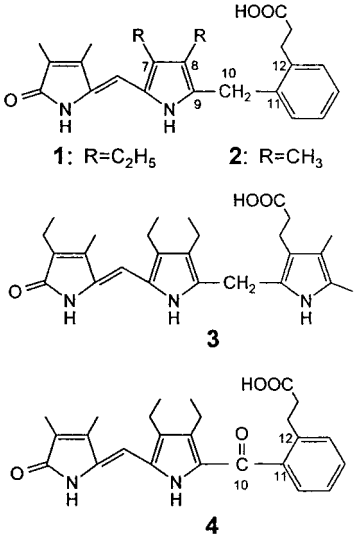

Results and Discussion

Synthesis

The target hemirubin (**1**) was prepared following $SnCl_4$-catalyzed Friedel–Crafts acylation of dipyrrinone **9** with acid chloride **7** to afford a 59% yield of 10-oxo-hemirubin **4** as its methyl ester (**4M**) (see Scheme 1). Saponification of **4M** gave an 85% yield of **4**, reduction of which by $NaBH_4$ in refluxing 2-propanol afforded the target (**1**) in 93% yield. Although acid chloride **7** was known from earlier work,[12] the dipyrrinone coupling partner (**9**) was not. It was prepared as outlined in Scheme 1 from two monopyrroles: **11** and **12** following decarboxylation of the coupled product **10**. Pyrrolinone **11** was known from earlier work;[9e] aldehyde **12** was prepared by oxidation of the 5-methyl group of pyrrole ester **13**[11] using ceric ammonium nitrate (CAN). Ester **13** was prepared from simple, inexpensive starting materials: reaction of 2-pentanone and propionic anhydride in the presence of $BF_3{\cdot}Et_2O$[15] gave condensation product **14** in 38% yield; reaction of **14** with base and Fischer–Knorr type condensation with the oxime of diethyl malonate using Zn and acetic acid[16] gave **13**. Simplified hemirubins **5** and **6**, which are incapable of intramolecular hydrogen bonding, served as comparison components and were prepared smoothly from dipyrrinone **9** and *o*-toluoyl chloride (**8**), as outlined in Scheme 1. The procedures parallel those used in the syntheses of **1** and **4**.

Constitutional structure

The structures of hemirubins **1** and **4**, and their methyl esters **1M** and **4M**, follow from the structures of the component

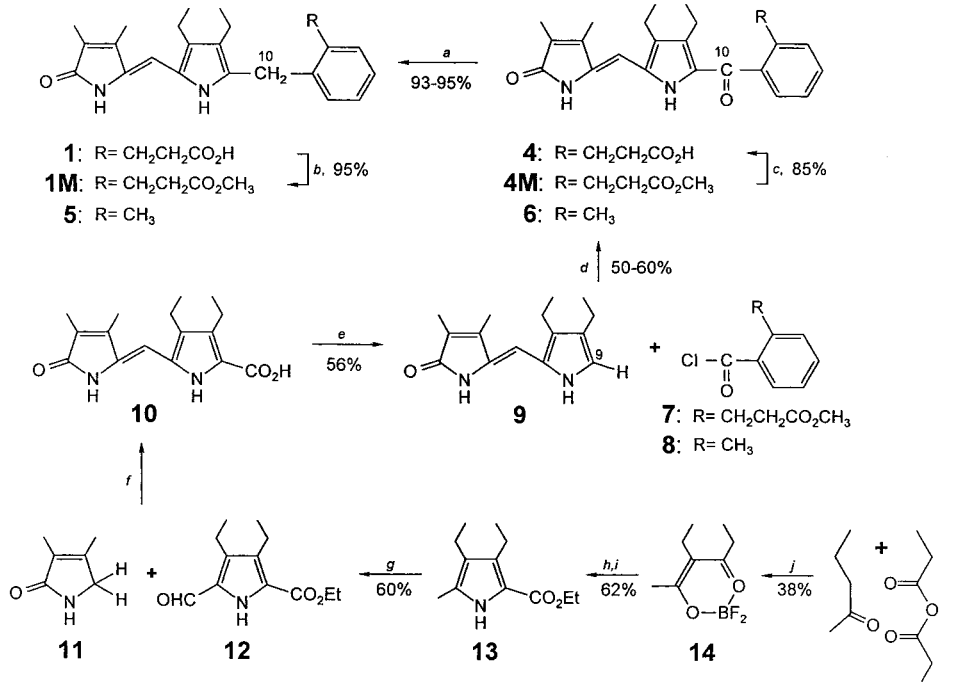

Scheme 1. *a* $NaBH_4$/2-propanol, refl.; *b* CH_3OH/H_2SO_4; *c* NaOH/aq. THF; *d* $SnCl_4/CH_2Cl_2$; *e* NaOAc–KOAc/Δ; *f* KOH/CH_3OH; *g* $Ce(NH_3)_2(NO_3)_4$/AcOH–H_2O; *h* NaOH; *i* HON = $C(CO_2Et)_2$/Zn–AcOH; *j* $BF_3{\cdot}Et_2O$.

Table 1. Comparison of ^{13}C NMR chemical shifts of hemirubin analogs

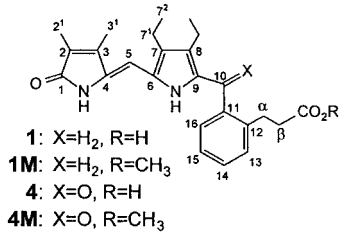

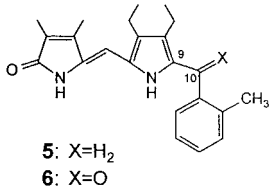

Carbon position	Chemical shift in $CDCl_3$[a]						
	9H-Dipyrrinone	**1**	**1M**	**5**	**4**	**4M**	**6**
1	174.5	174.7	173.5	173.9	175.7	175.7	174.0
2	130.4	128.8	129.0	128.8	137.5	137.5	135.9
3	142.6	142.0	142.1	142.0	141.6	141.7	141.9
4	129.9	129.5	131.5	131.6	128.3	130.1	130.4
5	101.4	101.1	100.6	100.7	99.1	96.0	96.6
6	126.0	123.0	123.1	123.1	127.3	129.9	130.3
7	123.8	123.9	123.7	123.7	129.6	129.9	130.4
8	124.5	134.6	132.3	132.3	135.3	135.4	134.7
9	120.5	122.8	122.0	122.0	129.3	128.7	128.6
10	–	27.2	30.0	30.3	188.1	187.8	187.0
11	–	138.4	138.2	135.8	141.4	140.1	140.3
12	–	138.4	137.7	138.0	139.7	138.1	136.9
13	–	130.4	129.4	129.8	129.2	129.6	125.4
14	–	128.8	128.7	128.3	127.3	126.1	127.0
15	–	126.6	126.6	126.0	125.4	127.1	129.6
16	–	126.3	126.6	126.0	130.1	130.0	130.6
α	–	24.6	27.9	19.6	26.0	28.3	19.4
β	–	32.0	34.6	–	34.4	35.3	–
CO_2R	–	179.1	173.8	–	177.9	173.7	–
2-CH_3	10.2	8.1	8.3	8.1	8.2	8.6	8.6
3-CH_3	8.5	9.7	9.9	9.8	9.7	9.9	9.9
7-CH_2	18.5	17.9	17.8	17.8	18.2	18.0	17.8
7-CH_3	17.9	17.3	17.3	17.3	17.2	17.3	17.3
8-CH_2	16.8	17.1	17.0	17.0	16.3	16.2	16.3
8-CH_3	15.1	16.8	15.6	15.7	15.6	15.7	15.9

[a] Chemical shifts in δ (ppm) downfield from the residual solvent resonances. Solutions were $\sim 5\times10^{-3}$ M.

dipyrrinone (**9**) and benzene derivative (**7**) used in their syntheses, and they are confirmed by ^{13}C NMR and $^{1}H\{^{1}H\}$-homonuclear Overhauser effect (NOE) spectroscopy (Table 1). The carbon chemical shift assignments of Table 1 were made by a combination of HMQC and HMBC techniques. The condensation product (**4**) of **5** and **6** shows the expected ten new signals from the aromatic ring component **6**, including the new C(10) ketone carbonyl at ~188 ppm. As expected, addition of the benzoyl group to dipyrrinone **9** caused the greatest ^{13}C NMR deshieldings in the carbons of the pyrrole ring of **4M** (or **4**). In addition, C(5) became more shielded, particularly in **4M** and much less so in **4**; and, at a remote site, C(2) became strongly deshielded. Conversion of **4M** to **1**, of C═O to CH_2, led to the expected strong shielding at C(10) in **1** and to other changes in ^{13}C NMR chemical shifts in **1** relative to **4**, especially in the pyrrole ring, but also at C(5) and C(2). Noticeable differences between certain signals in the free acids and their methyl esters (C(1), C(2), C(4), C(7), C(10) in **1** and **1M**; C(1), C(4), C(5), C(6) in **4** and **4M**) suggest differences in conformation in $CDCl_3$ solvent.

Comparisons (Table 1) with **5** and **6**, which are incapable of intramolecular hydrogen bonding, indicate a closer

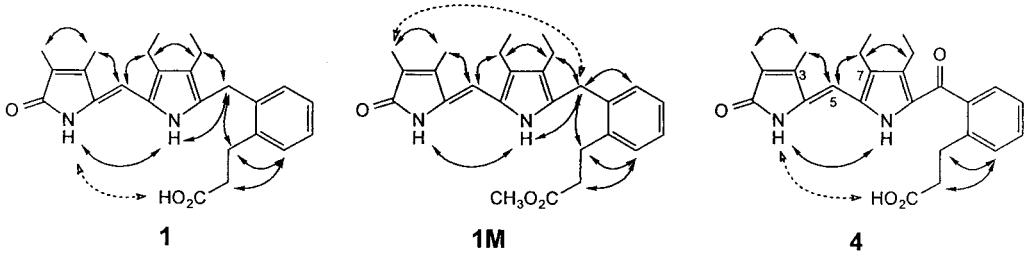

1 1M 4

Figure 2. Structurally significant NOEs found in **1**, **1M** and **4** are shown by solid, double-headed, curved arrows. Weak NOEs are shown by dashed, double-headed arrows.

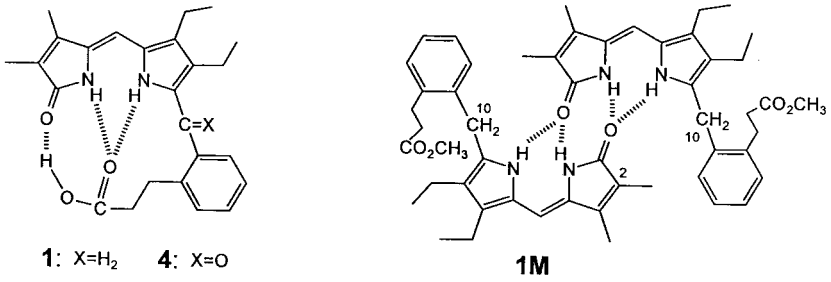

Figure 3. (Left) Intramolecularly hydrogen-bonded structures of **1** and **4**. (Right) Intermolecularly hydrogen-bonded dimeric structure of ester **1M**.

similarity in dipyrrinone chemical shifts of **6** with **4M** than with **4**, and of **5** with **1M** than with **1**. These comparisons are consistent with the notion that **1** and **4** engage in strong intramolecular hydrogen bonding in $CDCl_3$, and **1M** and **4M** might engage in weaker intramolecular hydrogen bonding, or in intermolecular hydrogen bonding.

Nuclear Overhauser effects and stereochemistry

Consistent with the constitutional structures of **1** and **4**, NOEs showed that the dipyrrinone unit retained the *syn-Z* configuration (Fig. 2). Thus, strong NOEs are seen between the pyrrole and lactam NHs and between the C(5)H and $C(3^1)CH_3$ and $C(7^1)CH_3$. Interestingly and significantly, NOEs are also found between the COOH and the lactam NHs of **1** and **4**, suggesting a close proximity between these groups. In **1M**, an NOE is found between the $C(2^1)CH_3$ and the C(10) CH_2, suggesting a close proximity between these groups. Such an NOE is not found in **1** and **4**. The data are consistent with intramolecular hydrogen bonding between the COOH and lactam groups in **1** and **4**, and with an intermolecularly hydrogen-bonded dimeric structure (Fig. 3) in **1M**.

Table 2. Comparison of hemirubin NH and COOH ^{1}H NMR chemical shifts (all spectra measured in 10^{-3} M solutions at 500 MHz and reported relative to residual solvent resonances)

Compounds[a]	δ (ppm) in $CDCl_3$			δ (ppm) in DMSO-d_6		
	Lactam	Pyrrole	Acid	Lactam	Pyrrole	Acid
9H-Dipyrrinone	11.05	10.41	–	9.72	10.48	–
1	10.58	8.58	13.47	9.75	10.33	12.12
1M	10.83	10.22	–	9.74	10.35	–
5	10.58	10.08	–	9.76	10.34	–
4	10.70	8.14	12.37	10.59	11.05	12.11
4M	9.06	8.43	–	10.58	11.04	–
6	9.66	9.46	–	10.58	11.01	–

[a] See Table 1 for structures.

^{1}H NMR and hydrogen bonding

Supporting evidence for intramolecular hydrogen bonding in **1** and **4** may be found from an examination of ^{1}H NMR chemical shifts of the lactam and pyrrole NHs (Table 2). In $(CD_3)_2SO$ these NH chemical shifts of **1**, **1M** and **5** are essentially identical and rather close to those of the parent 9*H*-dipyrrinone, as expected from previous studies, for monomeric structures solvated (and hydrogen-bonded) to DMSO. The NH chemical shifts of **4** and **4M** are nearly identical to those of **6**. In $CDCl_3$, however, where hydrogen bonding is promoted—either intramolecular or intermolecular between two dipyrrinones—the chemical shifts differ in a significant way. While the lactam NH becomes deshielded in **1**, **1M** and **5**, relative to its chemical shift in $(CD_3)_2SO$, the pyrrole NH becomes strongly shielded in **1** but only slightly shielded in **1M** and **5**. This behavior, noted earlier for various bilirubins and their dimethyl esters[10,16,17] and found in numerous dipyrrinone esters[10,17] and in

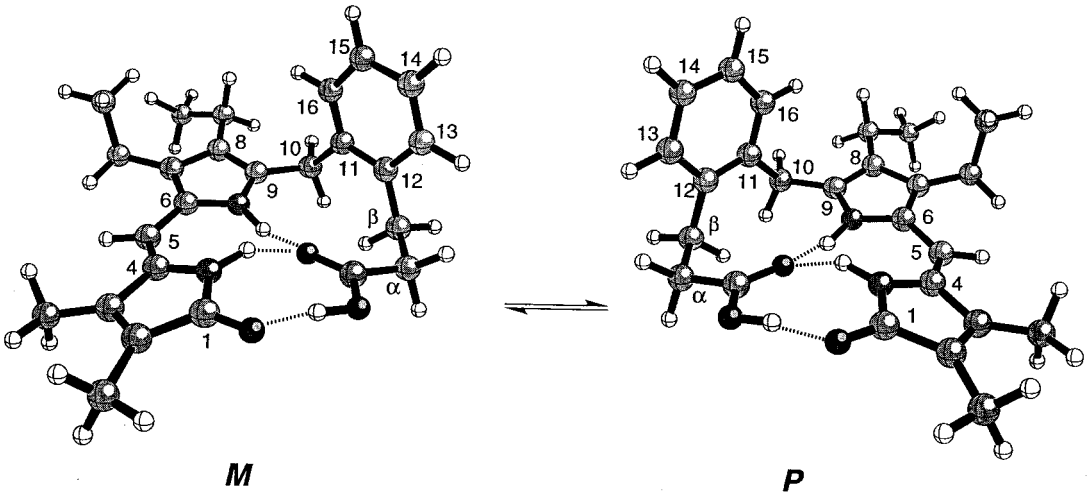

Figure 4. Ball and stick drawings for the global energy minimum conformational enantiomers of **1**. Hydrogen bonds are shown by hatched lines. See Table 6 for torsion angles, dihedral angles and hydrogen bond distances.

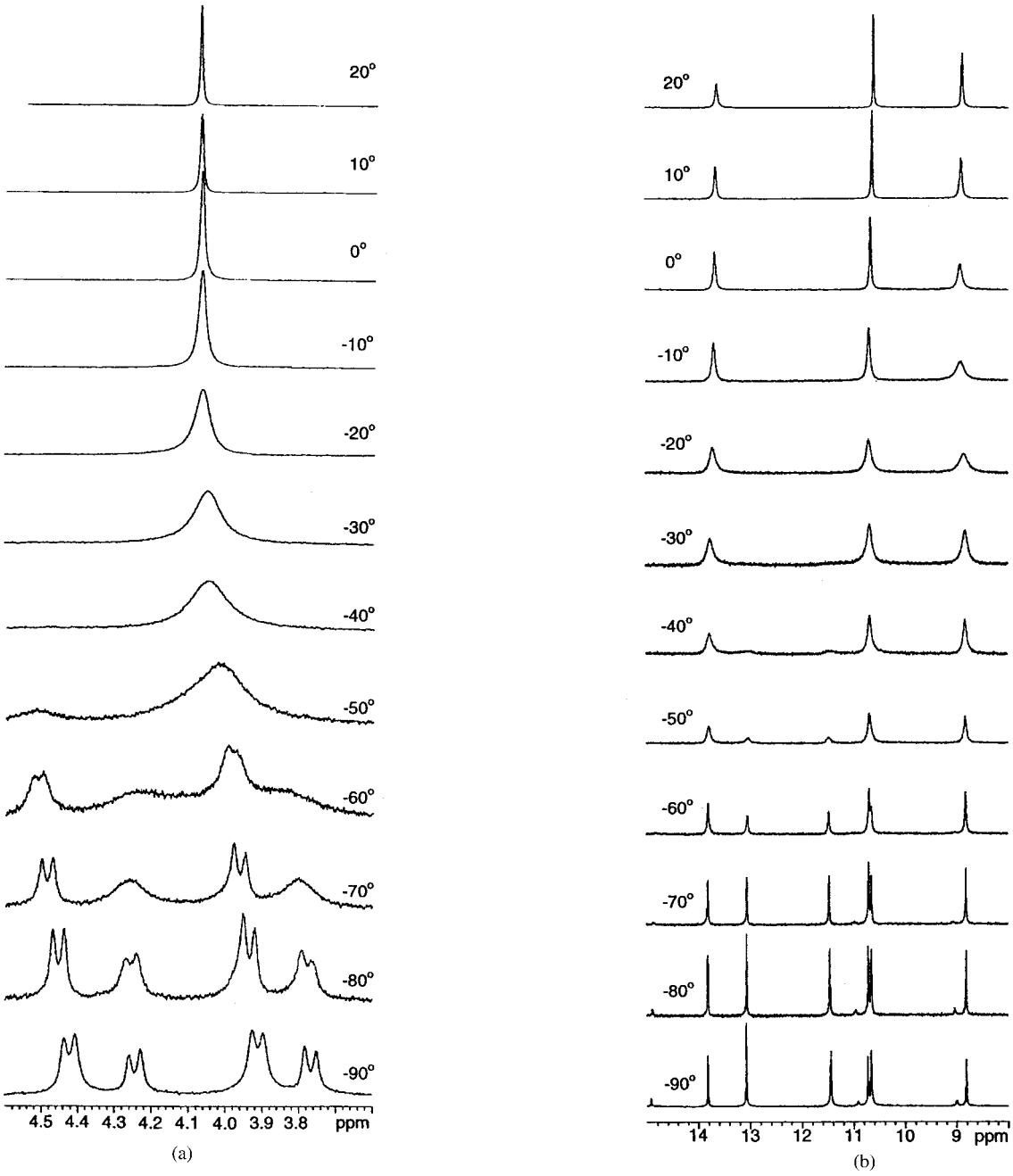

Figure 5. Variable low temperature ^{1}H NMR spectra of hemirubin **1** in CD_2Cl_2, showing (a) the region for the C(10) CH_2 resonance and (b) the region for the NH and COOH resonances.

recently reported tripyrrinone acids and esters,[11] is in accord with a predominantly intramolecularly hydrogen-bonded conformation of **1** and the presence of intermolecularly hydrogen-bonded planar dimer in **1M** and in **5**. In **1**, the intramolecularly hydrogen-bonded conformation (Fig. 3) does not have the phenyl-ring coplanar with the dipyrrinone but twisted out of plane at nearly right angles into either of two mirror image ridge-tile-shaped conformations (Fig. 4). In the ridge-tile conformation, the pyrrole NH lies above (or below) the benzene ring, which deshields the NH resonance.

The chemical shifts of **4** and **4M** are influenced somewhat by the C(10) carbonyl. Thus, in $(CD_3)_2SO$, the lactam and pyrrole NHs, while nearly identical and essentially the same as in **6**, are considerably deshielded relative to those of **1** and **1M**. In $CDCl_3$, the pyrrole NHs of **4** and **4M** exhibit strongly shielded (~8 ppm) chemical shifts, similar to that of **1** (but not **1M**). In fact, the pyrrole NH chemical shifts in $CDCl_3$ of **4** and **4M** are also much more deshielded than that of **6**, consistent with differing ridge-tile conformations. The lactam NH of **4** exhibits about the same shielding as that found in **1** and **1M** but differs considerably from that of **4M** and of **5**.

Molecular weights in solution from vapor pressure osmometry

There are only a few vapor pressure osmometry (VPO)

measurements of bilirubin pigments in nonpolar solvents—largely due to limited solubility of the pigment.[3] No VPO measurements of bilirubin acids have been performed, but bilirubin dimethyl ester (mol. wt. 616) was shown to exhibit a molecular weight of 850±20 in $CDCl_3$, 1100±30 in THF and 595±30 in CH_3OH.[3] These results indicate a dimer in THF, a monomer in CH_3OH, and a mixture of monomer and dimer in $CHCl_3$.

The molecular weights of **1**, **1M**, **4**, **4M**, **5** and **6** in $CHCl_3$ are shown in Table 3. Acids **1** and **4** are clearly monomeric, but the methyl analogs (**5** and **6**) are mainly dimeric. Esters **1M** and **4M** differ: surprisingly, **4M** is monomeric, while **1M** appears to be a mixture of monomer and dimer.

Variable low temperature ^{1}H NMR spectroscopic analysis

We prefer CD_2Cl_2 solvent to $CDCl_3$ for low temperature measurements, as it has a lower freezing point. The ^{1}H NMR spectrum of **1** at 20°C is similar to that in $CDCl_3$ and shows the expected sharp singlet for the C(10) CH_2 protons near 4.05 ppm (Fig. 5a) in addition to signals for the remaining hydrogens with essentially no change in chemical shift. We focused on the C(10) CH_2 signal; it is well-isolated from other proton resonances. It could be seen to broaden and shift upfield as the temperature is lowered. At approximately −50°C a new, broad signal appears near 4.5 ppm. Below −50°C, these two signals begin to sharpen and resolve into doublets, while shifting upfield slightly. At about −60°C a second set of broad signals appears and sharpens gradually into two doublets while moving slightly upfield as the temperature is lowered further to −90°C. We attribute these interesting changes to two distinct events: (i) a slowing down of conformational inversion (Fig. 4) between mirror image intramolecularly hydrogen-bonded conformers, and (ii) a monomer–dimer equilibrium. Evidence for the first may be found (Fig. 5a) when the conformational enantiomerism of Fig. 4 becomes slow on the NMR timescale and the C(10) hydrogens give clear evidence of their diastereotopicity. Note that the singlet near 4.05 ppm at 20°C broadens then splits into two doublets at ~−60°C, doublets (one near 4.42–4.52 ppm, the other near 3.92–4.00 ppm) which sharpen and remain of nearly equal intensity from −60−−90°. Evidence for the second, a monomer–dimer equilibrium may also be found in Fig. 5a

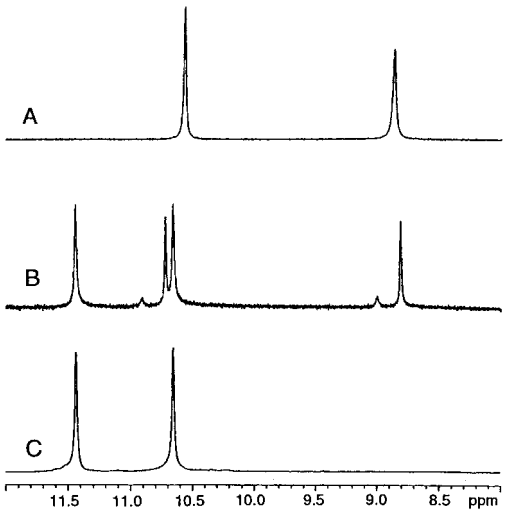

Figure 6. Partial ^{1}H NMR spectra in CD_2Cl_2 showing the region of NH resonance: (A) hemirubin **1** at +30°, (B) **1** at −90°C, and (C) hemirubin methyl ester **1M** at −90°C.

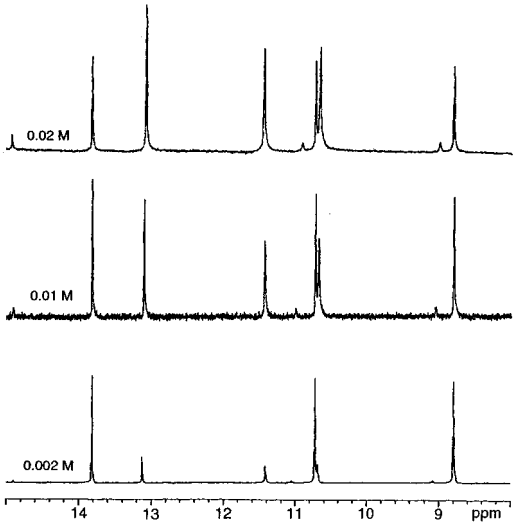

Figure 7. Partial ^{1}H NMR spectra of hemirubin **1** in CD_2Cl_2 at −90°C, and the influence of changing concentration on the lactam and pyrrole NH and COOH.

Table 3. Molecular weights of **1**, **1M**, **4**, **4M**, **5** and **6** in $CHCl_3$ from vapor pressure osmometry (solutions were 2.1×10^{-3}–9.5×10^{-3} M. VPO measurements were carried out at 45°C and calibrated vs. benzil (MW=210) in $CHCl_3$ (obs MW 220±15))

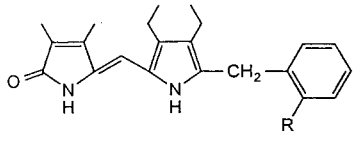

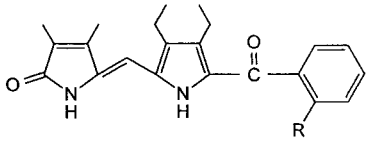

1	**1M**	**5**	**4**	**4M**	**6**
R =	R =	R =	R =	R =	R =
$CH_2CH_2CO_2H$	$CH_2CH_2CO_2CH_3$	CH_3	$CH_2CH_2CO_2H$	$CH_2CH_2CO_2CH_3$	CH_3
422 ± 10	526 ± 15	625 ± 25	422 ± 10	439 ± 30	675 ± 30
(406)[a]	(420)[a]	(348)[a]	(420)[a]	(434)[a]	(362)[a]

[a] Calculated molecular weight of the monomer.

Table 4. Monomer–dimer composition and K_{eq} for hemirubin **1** at low temperatures

Temperature (°C)	Monomer/dimer composition by integration[a] of ^{1}H NMR signals						K_{eq} based on ^{1}H NMR signals from		
	Acid COOH		Lactam NH		Pyrrole NH				
	Monomer	Dimer	Monomer	Dimer	Monomer	Dimer	Acid	Lactam	Pyrrole
−50	0.55	0.50	0.67	0.51	0.63	0.56	1.65	1.14	1.41
−60	0.81	0.50	1.00	0.55	1.05	0.55	0.76	0.55	0.58
−70	1.21	0.50	1.46	0.55	1.49	0.55	0.34	0.26	0.25
−80	1.45	0.41	1.82	0.45	1.80	0.44	0.195	0.14	0.14

[a] Integration performed using the NUTS NMR data processing program.

with the emergence of a second set of C(10) hydrogen signals at −60°C, signals (one near 4.25, the other near 3.78 ppm) which also appear as doublets.

The dimerization may be recognized more clearly by examining the NH and COOH chemical shifts of **1** in CD_2Cl_2 over the same temperature range. Figure 5b shows the anticipated three sharp singlets for each of lactams and pyrrole NH and COOH hydrogens, with chemical shifts nicely correlated with an intramolecularly hydrogen-bonded conformation, as discussed earlier for **1** in $CDCl_3$. Upon cooling, the signals begin to broaden near 0°C, and a new set of signals begins to emerge at approx. −40°C. Upon further cooling, the signals sharpen and one clearly sees (at −60°C) a new COOH signal near 13 ppm and new NH signals near 11.4 and 10.6 ppm. The chemical shifts of the original set of signals remains unchanged over the temperature range studied, and both sets of signals continue to sharpen upon further cooling. The new set of signals continues to grow, relative to the old set, and at ~80° yet another new set of very weak signals (~15, ~10.9 and ~9 ppm) appears.

Table 5. Thermodynamic data for the monomer–dimer equilibrium of hemirubin **1** (from van't Hoff plots (ln K_{eq} vs. $1/T$) the data of Table 4, with fitting parameters, R-values >0.998)

Energy[a]	Acid	Lactam	Pyrrole	Average
$\Delta G°$ (kcal/mol)	3.2	3.4	3.6	3.4
$\Delta H°$ (kcal/mol)	−5.6	−5.6	−5.7	−5.6
$\Delta S°$ (cal/mol)	−29.4	−30.2	−31.2	−30.3

[a] $\Delta G°$ and $\Delta H°$ ±0.5 kcal/mol; $\Delta S°$±1.0 cal/mol.

The lactam and pyrrole NH signals attributed to the dimer of **1** and seen in CD_2Cl_2 at −60−−90°C correlate nicely with those of its ester, **1M** in CD_2Cl_2 at −90°C (Fig. 6), which is thought to exist mainly as an intermolecularly hydrogen bonded dimer (as in Fig. 3). In further support of a monomer ⇄ dimer equilibrium of **1** in CD_2Cl_2 we observed a concentration dependence of the NH and COOH resonances (Fig. 7). At −90° and 0.002 M concentration, these resonances from the dimer are noticeably weaker than at 0.01 M, and at a 0.02 M concentration of **1**, they are at least as intense as the monomer. In addition, one may detect very weak signals near 15, 11 and 9 ppm. We assume that this weak set of new signals (seen at −80 and −90°C) might be associated with a different sort of dimer, one akin to the stacked dimer reported earlier for dipyrrinones such as xanthobilirubic acid with alkanoic acid β-substituents.[18]

Similar VT-NMR experiments on the 10-oxo analog **4** show no temperature dependence of the NH signals. However, as with **1** (Fig. 5a), we do observe variations in the CH_2 resonances of the propionic acid group. At +30°C one observes a broad 2H resonance for the α-protons of the $-C(\beta)H_2-C(\alpha)H_2-CO_2H$ segment, and a triplet for the β.

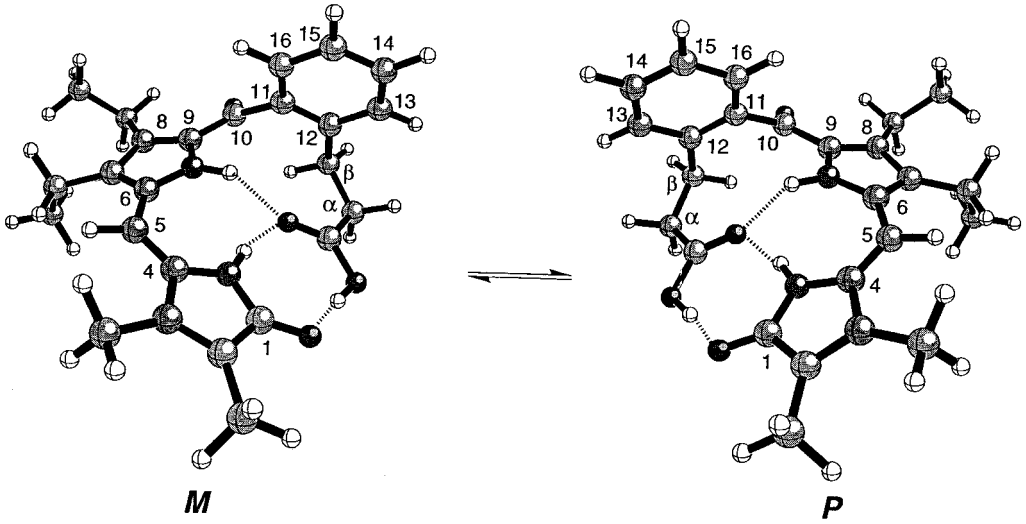

Figure 8. Ball and stick drawings for the global energy minimum conformational enantiomers of **4**. Hydrogen bonds are shown by hatched lines. See Table 6 for torsion angles, dihedral angles and hydrogen bond distances.

Table 6. Comparison of torsion and interplanar angles (°) and hydrogen bonding distances (Å) in global minimum conformations of hemirubins **1** and **4** with bilirubin (BR) and a 10-oxo-analog

Torsion (ϕ, ψ) and interplanar (θ) angles (°) and hydrogen bonding distances (d, Å)

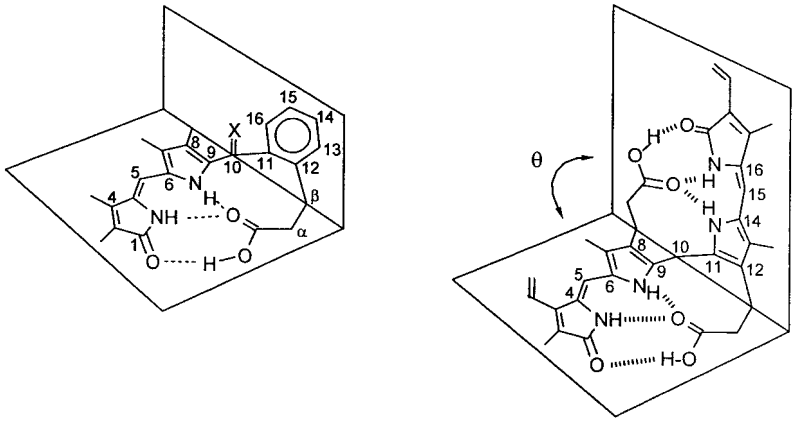

	1 (X=H_2)	**4** (X=O)	BR	10-oxo-MBR
ϕ_1 (N-9-10-11)	64	27	64	59
ϕ_2 (9-10-11-16) or (9-10-11-N)	66	60	64	60
ψ_1 (4-5-6-N)	−18	29	−17	−0.9
ψ_2 (N-14-15-16)	–	–	−17	−3.4
θ	97	76°	96°	88°
COOH···O═C (lactam) d	1.55	1.54	1.52	1.55
HO–C═O···HN (lactam) d	1.53	1.55	1.57	1.58
HO–C═O···NH (pyrrole) d	1.58	1.89	1.59	1.58

As the temperature is lowered, these signals broaden. One of the α-Hs coalescesces into the β-H_2 resonance, then both sharpen somewhat. The isolated α-H resonance is not sharp and thus not completely resolved at −90°C, and the other α-H (and two β-Hs) lie overlapped with the C(7)-ethyl CH_2 quartet, making detailed analysis very difficult.

Using VT NMR, we were able to sort out some thermodynamic parameters for the: (i) monomer ⇄ dimer equilibrium and (ii) ***M*** ⇄ ***P*** conformational enantiomerism of **1**. In (i) the exchange rate between monomer and dimer at low temperature is slow on the NMR timescale; thus, the equilibrium constant (K_{eq}) may be calculated at various low temperatures from the relative intensities of the pyrrole NH, the lactam NH or the acid proton signals (Table 4). The pyrrole and lactam data gave similar K_{eq} values; whereas the acid data gave a somewhat larger K_{eq}. Plots (van't Hoff) of ln K_{eq} vs. $1/T$ gave excellent linear fits and reasonably consistent data for $\Delta H°$ (∼−5.6 kcal/mol), $\Delta S°$ (∼−30.3 e.u.) and $\Delta G°$ (∼3.4 kcal/mol) (Table 5).

For the activation barrier to conformational inversion in **1** (Fig. 4), we used a line-shape analysis of the C(10) CH_2 resonance (Fig. 5a). From those data we could determine $k^{‡}$ over a wide temperature range in both CD_2Cl_2 and $CDCl_3$ solvents, and from the $k^{‡}$ values, using an Eyring plot (ln $k^{‡}/T$ vs. $1/f$), we determined: $\Delta G^{‡}_{298\ K}$ 9.94 kcal/mol, $\Delta H^{‡}$ −0.518 kcal/mol and $\Delta S^{‡}$ −35.1 cal/mol/deg for **1** in CD_2Cl_2; and $\Delta G^{‡}_{298\ K}$ 16.4 kcal/mol, $\Delta H^{‡}$ −9.08 kcal/mol and $\Delta S^{‡}$ −85.5 cal/mol/deg for **1** in $CDCl_3$. The nine points of the two Eyring plots graphed rather well to straight lines, with an excellent fit (R-values of >0.998). The computed $\Delta H^{‡}$ values are oddly solvent dependent; both $\Delta H^{‡}$ and $\Delta G^{‡}_{298\ K}$ are smaller in the more polar CD_2Cl_2 solvent. Previously, a $\Delta G^{‡}_{326\ K}$ ∼18 kcal/mol in $CDCl_3$ was determined for conformational enantiomerism in bilirubin,[19] corresponding to an inversion rate constant of k ∼7.2 s^{-1}. Since conformational inversion in bilirubin is thought to involve breaking at least three of six hydrogen bonds and conformational inversion in **1** involves breaking a minimum of one of three hydrogen bonds, the similarity in $\Delta G^{‡}$ values in $CDCl_3$ for these two pigments seems reasonable.

Conformational analysis by molecular dynamics computations

In order to gain further insight into the shape of **1** and **4**, molecular dynamics calculations (Sybyl)[20] gave two enantiomeric global minimum conformations for both. Those for **1** are shown in Fig. 4; those for **4** are very similar (Fig. 8) but show a smaller torsion angle about the C(10)–C(11) bond. The global minima are intramolecularly hydrogen-bonded, lying some 13 kcal/mol below the non-hydrogen-bonded global minima. The intramolecularly hydrogen-bonded global minimum conformation of **1** has various skeletal torsion angles and an interplanar dihedral angle very similar to that found in bilirubin (Table 6). Those for the oxo-analog **4** differ somewhat, especially at ϕ_2, which leads to a smaller θ—apparently a reflection of the change in geometry at C(10) from sp^3 to sp^2. This change in geometry also translates into a longer hydrogen bond between the carboxyl carbonyl oxygen and pyrrole NH in **4** than in **1**, thus predicting less effective hydrogen bonding in the former. The parameters for **4** are similar to those computed for 10-oxo-mesobilirubin-XIIIα.

Conformational energy maps[5] (Fig. 9) for enantiomerism in

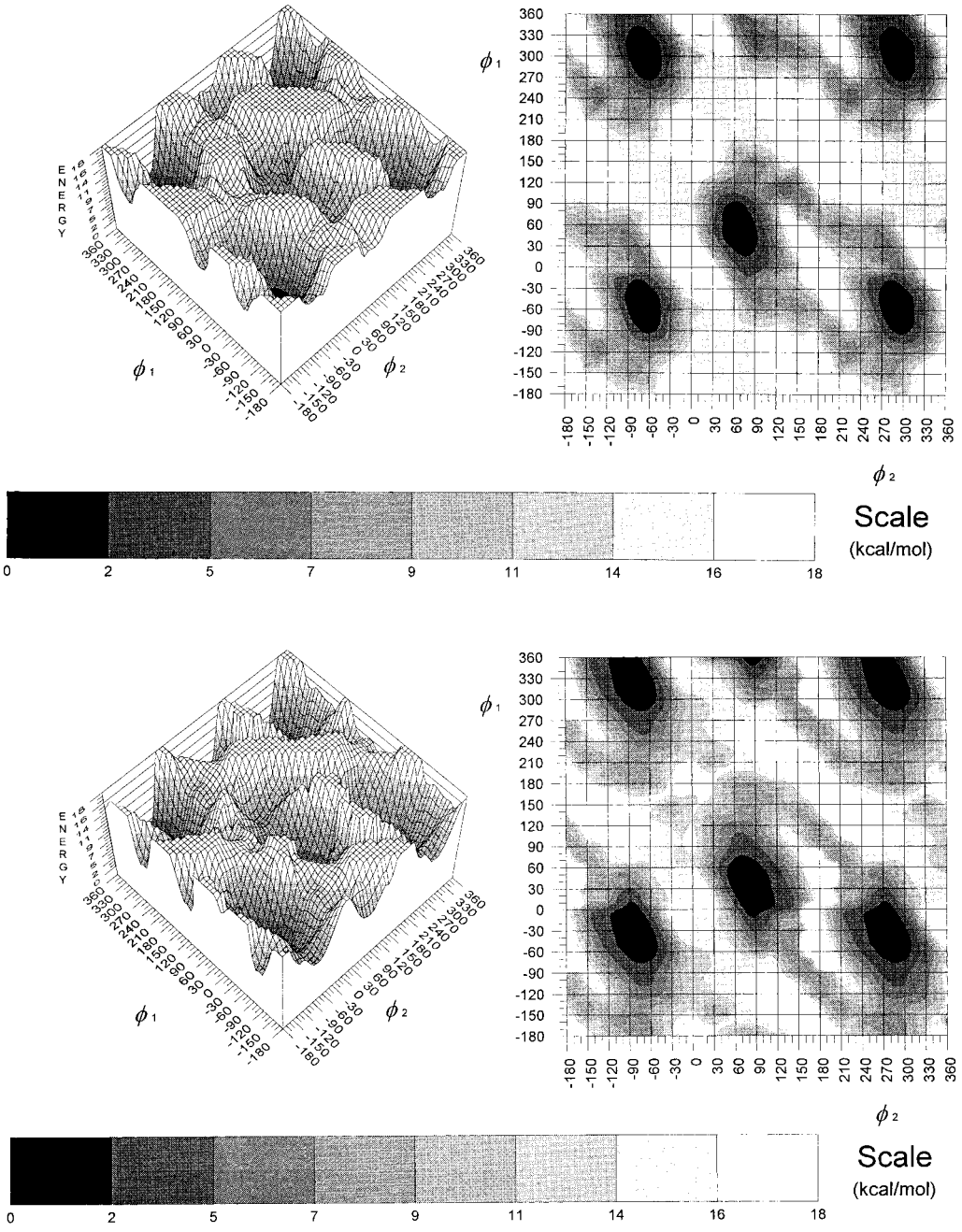

Figure 9. Potential energy surface (left) and contour map (right) for conformations of **1** (upper) and **4** (lower) generated by rotating their dipyrrinone and phenyl groups independently about the C(9)–C(10) and C(10)–C(11) bonds (ϕ_1 and ϕ_2, respectively). The energy scale is in kcal/mol. Isoenergetic global minima for **1** (set to 0 kcal/mol) are found near (ϕ_1, ϕ_2)=(60, 60°) (***P***-chirality) and near (ϕ_1, ϕ_2)=(− 70, −60°), (−70, 300°), (290, −60°), (290, 300°) (***M***-chirality).Local minima for **1** (∼6 kcal/mol above the global minima) are found near the (60, 60°) global minimum at (ϕ_1, ϕ_2)=(110, 130°), (250, 110°), (−60, 140°), (−110, 230°) and (250, −230°). Isoenergetic global minima (set to 0 kcal/mol) **4** are found near (ϕ_1, ϕ_2)=(30, 60°) (***P***-chirality) and near (ϕ_1, ϕ_2)=(330, −60°), (330, 350°), (−30, −60°) and (−30, 300°) (***M***-chirality). Local minima for **4** (∼9 kcal/mol above the global minimum at (30, 60°)) are found at (ϕ_1, ϕ_2)=(150, 130°), (230, 210°), (230, −150°), (−130, −150°) and (−130, 210°).

1 and **4** (Figs. 4 and 8) show small, deep valleys ringed by ridges and peaks, for rotations about the C(9)–C(10) and C(10)–C(11) bonds, corresponding to ϕ_1 and ϕ_2, respectively. The centrally-located valley corresponds to the ***M***-helical global energy minimum (Figs. 4 and 8); the four surrounding valleys correspond to the ***P***-helical global energy minima. Interconversion pathways between the ***M*** and ***P*** enantiomers may be found from such maps. For **1** (Fig. 9, top), we find the lowest energy path connects the global minimum at ϕ_1, ϕ_2=(+60, +60°) to its enantiomer at (−60, +300°) via conformers at (+60, +60°) ⇄ (+100, +120°) ⇄ (+60, +180°) ⇄ (+40, +260°) ⇄ (−10, +300°) ⇄ (−60, +300°). The saddle point at (+60, +180°) represents the highest energy conformer along the path, some 10 kcal/mol above the ***M*** and ***P***-helical enantiomers. Two somewhat higher barriers may be found along the different pathways (+60, +60°) ⇄ (+180, +60°) ⇄ (+220, +40°) ⇄ (+270, −10°) ⇄ (+300, −60°), and

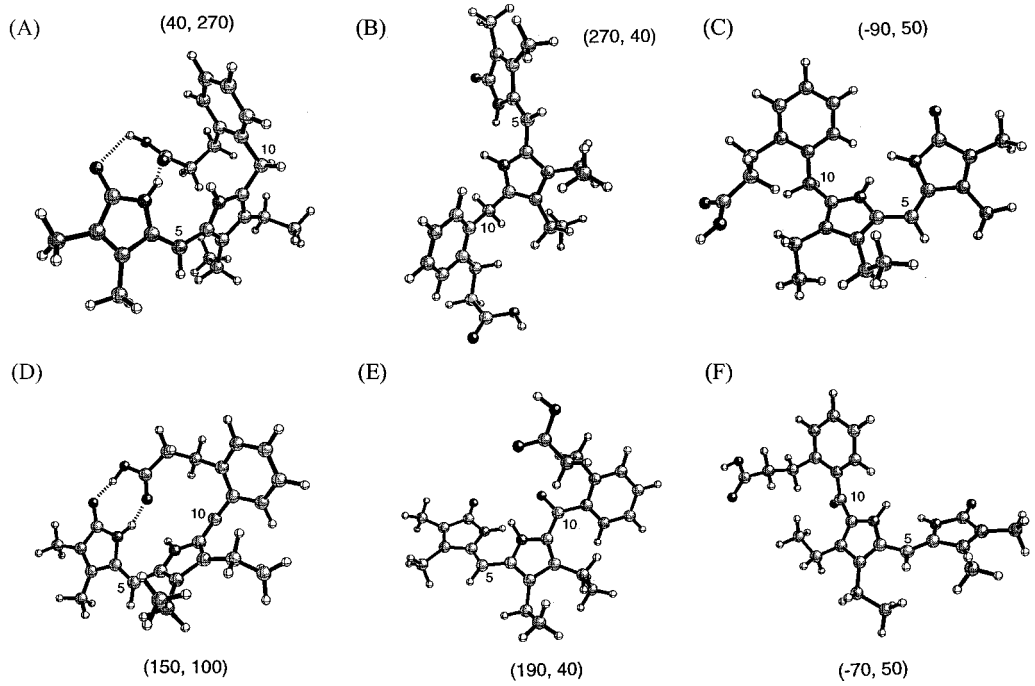

Figure 10. Ball and stick representations of the transition state structures lying on the lowest energy inter-conversion pathways for the ***M*** ⇄ ***P*** conformational enantiomerism of Figs. 4 and 8. Hemirubin **1** at (A) ϕ_1, $\phi_2 \sim +40, +270°$; (B) ϕ_1, $\phi_2 \sim +220, +40°$; and (C) ϕ_1, $\phi_2 \sim -90, +50°$. 10-oxo-hemirubin **4** at (D) ϕ_1, $\phi_2 \sim +150, +100°$; (E) ϕ_1, $\phi_2 \sim +190, +40°$; and (F) ϕ_1, $\phi_2 \sim -70, +50°$.

Table 7. UV-visible spectral data for hemirubin analogs and the parent 9*H*-dipyrrinone

	λ^{max} (ϵ^{max})[a] for						
Solvent	9*H*-Di-pyrrinone	**1**	**1M**	**5**	**4**	**4M**	**6**
C_6H_6	394(29,400)	430(28,500)	410(27,700)	410(27,500)	399(23,000) 420(19,100)	396(34,000) 415(28,800)	405(23,100) 429(21,600)
$CHCl_3$	389(25,400)	427(29,800)	407(29,600)	407(29,400)	401(17,900) 420(14,800)	400(27,200) 418(23,400)	402(28,800) 425(22,200)
CH_3OH	398(22,000)	414(32,000)	415(21,300)	413(39,600)	402(34,500) 423(30,200)	403(23,600) 423(20,800)	402(16,300) 424(15,000)
CH_3CN	384(29,700)	416(27,600)	402(29,600)	402(33,600)	392(22,200) 415(16,100)	394(37,200) 414(28,000)	394(17,500) 414(13,700)
$(CH_3)SO$	395(18,600)	412(33,900)	413(22,700)	413(19,300)	405(33,600) 428(32,700)	405(30,800) 428(23,400)	404(14,800) 428(13,600)

[a] λ^{max} in nm, ϵ in L·mol^{-1}.

(+60, +60°) ⇄ (−40, +80°) ⇄ (−90, +50°) ⇄ (−90, −30°) ⇄ (−60, −60°), both with barriers of ∼15 kcal/mol at transition points (+220, +40°) and (−90, +50°), respectively. For **4**, we find three low energy interconversion pathways on its conformational energy maps (Fig. 9 bottom). The lowest energy connects the global minimum at ϕ_1, ϕ_2=(+60, +60°) to its enantiomer at (−60, +300°) via conformers at (+60, +60°) ⇄ (+130, +90°) ⇄ (+150, +130°) ⇄ (+120, +170°) ⇄ (+30, +240°) ⇄ (+60, +300°). The saddle point at (+150, +130°) corresponds to the highest energy conformer along the path, ∼11 kcal/mol above the ***M*** and ***P***-helical global minima. Two other pathways, higher energy by 2–5 kcal/mol, are found: (i) (+60, +60°) ⇄ (+120, +70°) ⇄ (+190, +40°) ⇄ (+210, +20°) ⇄ (+240, 0°) ⇄ (300, −60°) and (ii) (+60, +60°) ⇄ (−20, +70°) ⇄ (−70, +50°) ⇄ (−70, −20°) ⇄ (−60, −60°). Route (i) crosses a barrier of ∼13 kcal/mol at (+190, +40°); route (ii) crosses a barrier of ∼15 kcal/mol at (−70, +50°). The structures of the transition state conformers at the saddle points are shown in Fig. 10.

Optical spectra

The UV-visible spectral data for hemirubins **1** and **1M** and their 10-oxo-analogs (**4** are **4M**) in solvents with a wide range of polarity are shown in Table 7. In polar solvents capable of engaging in hydrogen bonding, such as CH_3OH or $(CH_3)_2SO$, the long wavelength absorption of **1** has nearly the same λ^{max} and ϵ^{max} as its methyl ester (**1M**) and very similar to its *o*-xylyl analog. In nonpolar solvents, however, the spectra of **1** and **1M** are noticeably different, with **1** showing a strong bathochromic shift of λ^{max}; whereas, λ^{max} of **1M** and the *o*-xylyl analog are relatively unchanged. Although the spectral shifts do not unambiguously confirm an intramolecularly hydrogen bonded structure for **1**,

they are consistent with the ability of **1** to adopt a unique conformational structure in nonpolar solvents. The UV-visible spectral data for **4** and **4M** differ from those of **1** and **1M** due to the presence of the carbonyl group at C(10) and show the major long wavelength absorption near 400 nm, with an inflection or shoulder near 420–430 nm over the range of solvents studied. The spectra of **4** do not show the same sensitivity to change in solvent polarity, as seen in **1**. It may be noted that in both **4** and **4M**, the main absorption is bathochromically shifted upon changing from nonpolar solvents to those capable of hydrogen bonding; whereas in **1** it is hypsochromically shifted. The spectral shift seen in comparing the major absorption bonds of **1** to **1M** in nonpolar solvents is not evident in the spectra of **4** and **4M**.

Concluding Comments

The new hemirubin **1** with improved solubility in organic solvents is found to adopt preferentially either of two enantiomeric, intramolecularly hydrogen-bonded, ridge-tile-like conformation in nonpolar solvents. The interconversion barrier to conformational enantiomerism has been determined by variable low temperature ^{1}H NMR measurements to be $\Delta G^{\ddagger}_{298\ K}$ ~16 kcal/mol in $CDCl_3$ and ~10 kcal/mol in CD_2Cl_2. Variable low temperature ^{1}H NMR studies of **1** also reveal a monomer $\rightleftarrows$ dimer equilibrium, evident at low temperatures, with $\Delta G^{\ddagger}_{298\ K}$ (equiv.) ~3.4 kcal/mol. Spectroscopic (^{1}H NMR) and molecular modelling analyses suggest that the 10-oxo-analog (**4**) also adopts an intramolecularly hydrogen-bonded conformation. VPO measurements indicate that while **1**, **4** and **4M** are clearly monomeric in $CHCl_3$, **1M** shows the presence of some dimer at 45°C.

Experimental

General procedures

All ultraviolet-visible spectra were recorded on a Perkin–Elmer λ-12 spectrophotometer. Nuclear magnetic resonance (NMR) spectra were obtained on GE QE-300 or GE GN-300 spectrometers operating at 300 MHz, or on a Varian Unity Plus 500 MHz spectrometer in $CDCl_3$ solvent (unless otherwise specified). Chemical shifts were reported in δ ppm referenced to the residual $CHCl_3$ ^{1}H signal at 7.26 ppm and ^{13}C signal at 77.0 ppm. Heteronuclear Multiple Quantum Coherence (HMQC) and Heteronuclear Multiple Bond Correlation (HMBC) spectra were used to assign ^{13}C NMR spectra. Vapor Pressure Osmometry (VPO) measurements were performed using an Osmomat 070 (Gonotec, Berlin, Germany) in $CHCl_3$ at 45°C with benzil used for calibration. Melting points were taken on a MelTemp capillary apparatus and are uncorrected. Combustion analyses were carried out by Desert Analytics, Tucson, AZ. Analytical thin layer chromatography was carried out on J. T. Baker silica gel IB-F plates (125 μ layers). Flash column chromatography was carried out using Woelm silica gel F, thin layer chromatography grade. Radial chromatography was carried out on Merck Silica Gel PF_{254} with gypsum preparative layer grade, using a Chromatotron (Harrison Research, Inc., Palo Alto, CA). Spectral data were obtained in spectral grade solvents (Aldrich or Fischer). Ceric ammonium nitrate was from Aldrich, and stannic chloride was from Baker. Dichloromethane, methanol, DMSO, acetic acid, tetrahydrofuran, hexane, and 2-propanol were from Fischer, and 2-pentanone and propionic anhydride were from Acros.

***o*-(Methoxycarbonylethyl)benzoyl chloride** (**7**) was prepared from β-naphthol as described previously.[12] ***o*-Toluoyl chloride** (**8**) was prepared by reaction of *o*-toluic acid with $SOCl_2$.

9-[2-(Carboxyethyl)benzyl]-3,4-dimethyl-7,8-diethyl-dipyrrinone (1). Dipyrrinone (**4M**) (200 mg, 0.46 mmols) and 200 mL of 2-propanol were placed in a 100 mL round-bottom flask equipped for magnetic stirring. Sodium borohydride (100 mg, 1.7 mmols) was added, and the reaction mixture was heated at reflux for 2 h. The hot reaction mixture was poured into 100 mL of ice water and the solution was acidified with 10% aq. HCl. The suspension was extracted with dichloromethane (3×50 mL), and the combined organic extracts were washed with water (3×100 mL) and dried over Na_2SO_4 (anhydr.). The solvent was removed (Rotovap), and the crude product was purified by radial chromatography (97:3 by vol. CH_2Cl_2:MeOH) and recrystallized from CH_2Cl_2–hexane to give 0.182 g of **1**, 93% yield. It had mp 209–10°C; IR (KBr) ν 3440, 3351, 2964, 2928, 2869, 1707, 1664, 1636, 1459, 1373, 1247, 1181, 942, 735, 694 cm^{-1}; ^{1}H NMR ($CDCl_3$, 500 MHz) δ 1.18 (t, *J*=7.5 Hz, 3 H), 1.24 (t, *J*=7.5 Hz, 3 H), 1.84 (s, 3 H), 2.05 (s, 3 H), 2.58 (q, *J*=7.5 Hz, 2 H), 2.61 (q, *J*=7.5 Hz, 2 H), 2.97 (t, *J*=7.5 Hz, 2 H), 3.07 (t, *J*=7.5 Hz, 2 H), 4.10 (s, 2 H), 6.07 (s, 1 H), 7.02 (d, *J*=7.5 Hz, 1 H), 7.05 (t, *J*=7.5 Hz, 1 H), 7.14 (t, *J*=7.5 Hz, 1 H), 7.23 (d, *J*=7.5 Hz, 2 H), 8.85 (bs, 1 H), 10.58 (bs, 1 H), 13.47 (bs, 1 H) ppm; ^{1}H NMR (DMSO-d_6, 500 MHz) δ 0.84 (t, *J*=7.5 Hz, 3 H), 1.08 (t, *J*=7.5 Hz, 3 H), 1.76 (s, 3 H), 2.06 (s, 3 H), 2.24 (q, *J*=7.5 Hz, 2 H), 2.46 (t, *J*=7.5 Hz, 2 H), 2.51 (q, *J*=7.5 Hz, 2 H), 2.91 (t, *J*=7.5 Hz, 2 H), 3.95 (s, 2 H), 5.95 (s, 1 H), 6.78 (d, *J*=7.5 Hz, 1 H), 7.11 (m, 3 H), 9.75 (bs, 1 H), 10.33 (bs, 1 H), 12.12 (bs, 1 H) ppm; with ^{13}C NMR data in Table 1; and UV-vis data in Table 7. Anal. Calcd for $C_{25}H_{30}N_2O_3$ (406.2): C, 73.85; H, 7.44; N, 6.89. Found: C, 73.57; H, 7.53; N, 6.87.

9-[2-(Methoxycarbonylethyl)benzyl]-3,4-dimethyl-7,8-diethyl-dipyrrinone (1M). Dipyrrinone (**1**) (27 mg, 0.067 mmols) and 50 mL of methanol were added to a 100 mL round-bottom flask equipped for magnetic stirring. Ten milliliters of 10% aq. H_2SO_4 were added to the solution dropwise over 5 min, and the reaction mixture was heated at reflux for 1 h. The reaction mixture was cooled to room temperature, taken up in dichloromethane (50 mL), and washed with water (2×100 mL) and saturated aq. sodium bicarbonate solution (2×100 mL). The organic extract was dried over Na_2SO_4 (anhydr.) and the solvent removed (Rotovap). The residue was purified by radial chromatography (97:3 by vol. CH_2Cl_2:MeOH) and recrystallized from CH_2Cl_2–hexane) to give the desired product (27 mg) in 95% yield. It had mp 197–199°C; IR (KBr) ν 3360, 2964, 2929, 1742, 1665, 1631, 1462, 1369, 1277, 1178, 943, 756,

692 cm^{-1}; ^1H NMR ($CDCl_3$, 500 MHz) δ 1.00 (t, J=7.5 Hz, 3 H), 1.28 (t, J=7.5 Hz, 3 H), 1.78 (s, 3 H), 2.20 (s, 3 H), 2.41 (q, J=7.5 Hz, 2 H), 2.61 (q, J=8.0 Hz, 2 H), 2.68 (q, J=7.5 Hz, 2 H), 3.16 (t, J=8.0 Hz, 2 H), 3.77 (s, 3 H), 4.30 (s, 2 H), 6.14 (s, 1 H), 7.15–7.25 (m, 4 H), 10.22 (bs, 1 H), 10.83 (bs, 1 H) ppm; ^1H NMR (DMSO-d_6, 500 MHz) δ 0.80 (t, J=7.5 Hz, 3 H), 1.07 (t, J=7.5 Hz, 3 H), 1.77 (s, 3 H), 2.06 (s, 3 H), 2.22 (q, J=7.5 Hz, 2 H), 2.46 (m, 4 H), 2.93 (t, J=8.0 Hz, 2 H), 3.55 (s, 3 H), 3.95 (s, 2 H), 5.94 (s, 1 H), 6.84 (d, J=7.5 Hz, 1 H), 7.14 (m, 3 H), 9.74 (bs, 1 H), 10.33 (bs, 1 H) ppm; with ^{13}C NMR data in Table 1; and UV-vis data in Table 7. Anal. Calcd for $C_{26}H_{32}N_2O_3$ (420.2): C, 74.24; H, 7.67; N, 6.66. Found: C, 73.98; H, 7.49; N, 6.54.

9-[2-(Carboxyethyl)benzoyl]-3,4-dimethyl-7,8-diethyl-dipyrrinone (4). Dipyrrinone **4M** (73 mg, 0.16 mmols) and 50 mL of THF were placed in a 100 mL round-bottom flask equipped for magnetic stirring. Ten milliliters of 2 M NaOH (aq.) were added; then the mixture was heated at reflux for 3 h, quenched by pouring into ice–water and acidified with 10% aq. HCl. The suspension was extracted into dichloromethane (3×70 mL) and washed with water (3×100 mL). The combined organic extracts were dried over anhydr. sodium sulfate and evaporated (Rotovap). The residue was purified by radial chromatography (97:3 by vol. CH_2Cl_2:MeOH) and recrystallized from CH_2Cl_2–hexane). Pure acid **4** (70 mg) was obtained in 85% yield. It had mp 237–238°C; IR (KBr) ν 3365, 3194, 2966, 2921, 1688, 1602, 1429, 1398, 1290, 1158, 1024, 928, 758 cm^{-1}; ^1H NMR ($CDCl_3$, 500 MHz) δ 1.18 (t, J=7.5 Hz, 3 H), 1.27 (t, J=7.5 Hz, 3 H), 1.85 (s, 3 H), 2.08 (s, 3 H), 2.55 (q, J=7.5 Hz, 2 H), 2.84 (bs, 2 H), 2.90 (bs, 2 H), 3.07 (bs, 2 H), 6.05 (s, 1 H), 7.10–7.40 (m, 4 H), 8.14 (bs, 1 H), 10.70 (bs, 1 H), 12.37 (bs, 1 H) ppm; ^1H NMR (DMSO-d_6, 500 MHz) δ 0.77 (t, J=7.5 Hz, 3 H), 1.05 (t, J=7.5 Hz, 3 H), 1.80 (s, 3 H), 2.06 (m, 4 H), 2.09 (s, 3 H), 2.52 (t, J=7.5 Hz, 2 H), 2.79 (t, J=7.5 Hz, 2 H), 5.93 (s, 1 H), 7.30–7.50 (m, 4 H), 10.59 (bs, 1 H), 11.05 (bs, 1 H), 12.11 (bs, 1 H) ppm; with ^{13}C NMR data in Table 1; and UV-vis data in Table 7. Anal. Calcd for $C_{25}H_{28}N_2O_4$ (420.2): C, 71.39; H, 6.76; N, 6.66. Found: C, 71.12; H, 6.64; N, 6.52.

9-[2-(Methoxycarbonylethyl)benzoyl]-3,4-dimethyl-7,8-diethyl-dipyrrinone (4M). 3,4-Dimethyl-7,8-diethyl dipyrrinone (**9**) (0.300 g, 1.22 mmols) and 100 mL of dichloromethane were added to a 500 mL round-bottom flask equipped for magnetic stirring. The solution was cooled in an ice bath for 20 min with stirring; then a solution of acid chloride **7** (1.0 g, 4.4 mmols) and $SnCl_4$ (4.5 g, 17.3 mmols) in 100 mL of dichloromethane was added in one portion. The reaction mixture was stirred for 1.5 h at room temperature then poured into a mixture of conc. HCl (200 mL) and 100 g of ice and stirred for 2 h. The organic layer was separated, and the aqueous layer extracted with dichloromethane (2×100 mL). The combined organic extracts were washed with sat. aq. $NaHCO_3$ (2×200 mL) then with water (400 mL), and dried over anhydr. Na_2SO_4. The solvent was removed (Rotovap), and the crude product was purified by radial chromatography (97:3 by vol. CH_2Cl_2:MeOH) and recrystallized from CH_2Cl_2–hexane to afford 0.313 g, 59% of **4M**. It had mp 167–168°C; IR (KBr) ν 3344, 2966, 2872, 1735, 1660, 1607, 1431, 1405, 1282, 1168, 928, 758, 690, 668 cm^{-1}; ^1H NMR ($CDCl_3$, 500 MHz) δ 0.96 (t, J=7.5 Hz, 3 H), 1.15 (t, J=7.5 Hz, 3 H), 1.91 (s, 3 H), 2.10 (s, 3 H), 2.37 (q, J=7.5 Hz, 2 H), 2.51 (q, J=7.5 Hz, 2 H), 2.67 (t, J=7.5 Hz, 2 H), 3.00 (t, J=7.5 Hz, 2 H), 3.62 (s, 3 H), 6.07 (s, 1 H), 7.26–7.40 (m, 4 H), 8.43 (bs, 1 H), 9.06 (bs, 1 H) ppm; ^1H NMR (DMSO-d_6, 500 MHz) δ 0.77 (t, J=7.5 Hz, 3 H), 1.05 (t, J=7.5 Hz, 3 H), 1.80 (s, 3 H), 2.06 (q, J=7.5 Hz, 4 H), 2.09 (s, 3 H), 2.60 (t, J=7.0 Hz, 2 H), 2.83 (t, J=7.0 Hz, 2 H), 3.55 (s, 3 H), 5.93 (s, 1 H), 7.31–7.45 (m, 4 H), 10.58 (bs, 1 H), 11.04 (bs, 1 H) ppm; with ^{13}C NMR data in Table 1; and UV-vis data in Table 7. Anal. Calcd for $C_{26}H_{30}N_2O_4$ (434.2): C, 71.85; H, 6.96; N, 6.45. Found: C, 71.45; H, 6.77; N, 6.33.

9-(2-Methylbenzyl)-3,4-dimethyl-7,8-diethyl-dipyrrinone (5). Dipyrrinone **6** (97 mg, 0.27 mmols) and 200 mL of 2-propanol were placed in a 100 mL round-bottom flask equipped for magnetic stirring. Sodium borohydride (100 mg, 1.7 mmols) was added, and the reaction mixture was heated at reflux for 2 h. The hot reaction mixture was poured into 100 mL of ice–water and the solution was acidified with 10% aq. HCl. The suspension was extracted with dichloromethane (3×50 mL), and the combined organic extracts were washed with water (3×100 mL) and dried over Na_2SO_4 (anhydr.). The solvent was removed (Rotovap), and the crude product was purified by radial chromatography (97:3 by vol. CH_2Cl_2:MeOH) and recrystallized from CH_2Cl_2–hexane to give 93 mg of **5**, 92%. It had mp 258–259°C; IR (KBr) ν 3469, 3348, 2967, 2915, 1666, 1636, 1457, 1369, 1274, 1179, 739, 694 cm^{-1}; ^1H NMR ($CDCl_3$, 500 MHz) δ 0.91 (t, J=7.5 Hz, 3 H), 1.16 (t, J=7.5 Hz, 3 H), 1.62 (s, 3 H), 2.06 (s, 3 H). 2.33 (s, 3 H), 2.57 (q, J=7.5 Hz, 2 H), 2.71 (q, J=7.5 Hz, 2 H), 4.10 (s, 2 H), 6.11 (s, 1 H), 6.90–7.25 (m, 4 H), 10.08 (bs, 1 H), 10.85 (bs, 1 H), ppm; ^1H NMR (DMSO-d_6, 500 MHz) δ 0.86 (t, J=7.5 Hz, 3 H), 1.08 (t, J=7.5 Hz, 3 H), 1.76 (s, 3 H), 2.06 (s, 3 H), 2.24 (q, J=7.5 Hz, 2 H), 2.33 (s, 3 H), 2.52 (q, J=7.5 Hz, 2 H), 3.87 (s, 2 H), 5.95 (s, 1 H), 6.78–7.23 (m, 4 H), 9.76 (bs, 1 H), 10.34 (bs, 1 H), ppm; with ^{13}C NMR data in Table 1; and UV-vis data in Table 6. Anal. Calcd for $C_{23}H_{28}N_2O$ (348.2): C, 79.26; H, 8.10; N, 8.04. Found: C, 79.27; H, 8.19; N, 8.26.

9-(2-Methylbenzoyl)-3,4-dimethyl-7,8-diethyl-dipyrrinone (6). 3,4-Dimethyl-7,8-diethyl dipyrrinone (**9**) (0.30 g, 1.22 mmols) and 100 mL of dichloromethane were added to a 500 mL round-bottom flask equipped for magnetic stirring. The solution was cooled in an ice bath for 20 min with stirring; then a solution of acid chloride (**8**) (0.6 g, 3.9 mmols) and $SnCl_4$ (2.4 g, 9.2 mmols) in 100 mL of dichloromethane was added in one portion. The reaction mixture was stirred for 1.5 h at room temperature then poured into a mixture of conc. HCl (200 mL) and 100 g of ice and stirred for 2 h. The organic layer was separated, and the aqueous layer extracted with dichloro-methane (2×100 mL). The combined organic extracts were washed with sat. aq. $NaHCO_3$ (2×200 mL) then with water (400 mL), and dried over anhydr. Na_2SO_4. The solvent was removed (Rotovap), and the crude product was purified by radial chromatography (97:3 by vol. CH_2Cl_2:MeOH) and recrystallized from CH_2Cl_2–hexane to afford 0.223 g, 50% of **6**. It had mp 237°C; IR (KBr) ν 3460, 3351, 2967, 2930,

1659, 1609, 1431, 1403, 1275, 1166, 926, 762, 728, 682 cm^{-1}; ^1H NMR ($CDCl_3$, 500 MHz) δ 0.82 (t, J=7.5 Hz, 3 H). 1.13 (t, J=7.5 Hz, 3 H), 1.94 (s, 3 H), 2.10 (s, 3 H), 2.13 (q, J=7.5 Hz, 2 H), 2.32 (s, 3 H), 2.50 (q, J=7.5 Hz, 2 H), 5.96 (s, 1 H), 7.26–7.40 (m, 4 H), 9.46 (bs, 1 H), 9.66 (bs, 1 H) ppm; ^1H NMR (DMSO-d_6, 500 MHz) δ 0.77 (t, J=7.5 Hz, 3 H), 1.05 (t, J=7.5 Hz, 3 H), 1.80 (s, 3 H), 2.08 (s, 3 H), 2.10 (q, J=7.5 Hz, 2 H), 2.24 (s, 3 H), 2.49 (q, J=7.5 Hz, 2 H), 5.93 (s, 1 H), 7.25–7.50 (m, 4 H), 10.58 (bs, 1 H), 11.01 (bs, 1 H) ppm; with ^{13}C NMR data in Table 1; and UV-vis data in Table 7. Anal. Calcd for $C_{23}H_{26}N_2O_2$ (362.2): C, 76.20; H, 7.23; N, 7.73. Found: C, 76.05; H, 7.12; N, 7.63.

2,3,-Dimethyl-7,8-diethyl-9*H*-dipyrrinone (9). 3,4-Diethyl-5-formyl-2-carboethoxy-*1H*-pyrrole (**12**) (6.0 g, 27 mmols), 3,4-dimethyl-*1H*-pyrrolin-2-one (**11**) (3.0 g, 27 mmols) and 50 mL of methanol were placed in a 500 mL round-bottom flask equipped for magnetic stirring. 200 milliliters of 4 M KOH (aq.) were added, and the reaction mixture was heated at reflux for 4 h then chilled in an ice bath for 30 min followed by acidification with HCl (conc) to ~pH 3. The resultant solid product (**10**) was collected by filtration (vacuum), washed with water (100 mL), and dried in vacuo. The resulting powder was placed in a 500 mL round-bottom flask and mixed with 3.0 g of potassium acetate and 3.0 g of sodium acetate trihydrate which had been ground with a mortar and pestle until intimately mixed. The solid mixture was heated to ~160° at which time it melted with the evolution of CO_2. The temperature was maintained at ~160° until the evolution of CO_2 ceased, ~10 min The reaction mixture was cooled to room temperature and 400 mL of water was added followed by vigorous stirring for 1 h. The product was collected by filtration (vacuum) and triturated with cold acetone (50 mL) to give pure dipyrrinone **9**, 2.1 g, 56% yield. It had mp 203–204°C; IR (KBr) ν 3397, 3193, 3150, 2953, 2910, 1648, 1507, 1398, 1267, 1174, 1114, 939, 793, 750, 690 cm^{-1}; ^1H NMR ($CDCl_3$, 500 MHz) δ 1.13 (t, J=7.5 Hz, 3 H), 1.21 (t, J=7.5 Hz, 3 H), 1.94 (s, 3 H), 2.13 (s, 3 H), 2.52 (q, J=7.5 Hz, 2 H), 2.82 (q, J=7.5 Hz, 2 H), 6.20 (s, 1 H), 6.86 (d, J=2.5 Hz, 2 H), 10.41 (bs, 1 H) 11.05 (bs, 1 H) ppm; ^1H NMR (DMSO-d_6, 500 MHz) δ 1.04 (t, J=7.5 Hz, 3 H), 1.13 (t, J=7.5 Hz, 3 H), 1.77 (s, 3 H), 2.05 (s, 3 H), 2.37 (q, 7.5 Hz, 2 H), 2.47 (q, J=7.5 Hz, 2 H), 5.94 (s, 1 H), 6.72 (d, J=2.5 Hz, 2 H), 9.72 (bs, 1 H) 10.48 (bs, 1 H) ppm; and ^{13}C NMR ($CDCl_3$, 125 MHz) δ 8.52, 10.18, 13.10, 16.78, 17.94, 18.47, 101.36, 120.54, 123.83, 124.34, 125.94, 129.90, 130.41, 142.63, 174.46 ppm; The UV-vis data are in Table 7. Anal. Calcd for $C_{215}H_{20}N_2O$ (244.2): C, 73.72; H, 8.26; N, 11.47. Found: C, 73.93; H, 8.19; N, 11.19.

3,4-Diethyl-5-formyl-2-carboethoxy-1*H*-pyrrole (12). To a 1 L round-bottom flask equipped for magnetic stirring was added 5-methyl-3,4-diethyl-2-carboethoxy-*1H*-pyrrole (**13**) (7.0 g, 33 mmols), 120 mL of tetrahydrofuran, 240 mL of acetic acid, and 200 mL of water. The reaction mixture was cooled in a ice bath for 30 min; then ceric ammonium nitrate (73.0 g, 132 mmols) was added in one portion, and the mixture was stirred at room temperature for 2 h. The reaction mixture was extracted with dichloromethane (3×150 mL) and the combined organic extracts were washed with water (3×400 mL), sat. aq. sodium bicarbonate (2×300 mL), and dried over sodium sulfate (anhydr.). The solvent was removed (Rotovap) to yield an oily residue which was crystallized from methanol–water to give 6.0 g of solid **12** (80%). It had mp 50–51°C (lit.[5] mp 53°C); and ^1H NMR ($CDCl_3$, 300 MHz) 1.15 (t, J=7.5 Hz, 3 H), 1.23 (t, J=7.5 Hz, 3 H), 1.37 (t, J=7.5 Hz, 3 H), 2.73 (q, J=7.5 Hz, 4 H), 4.36 (q, J=7.5 Hz, 2 H), 9.52 (bs, 1 H), 9.78 (bs, 1 H) ppm.

5-Methyl-3,4-diethyl-2-carboethoxy-1*H*-pyrrole (13). To a 250 mL round-bottom flask equipped for magnetic stirring was added 3-ethyl-2,4-hexanedione-O^2, O^4-difluoroboronate (9.0 g, 47 mmols) and 25 mL of methanol. A solution of 50% aqueous NaOH was added to adjust the pH to ~9.0. The reaction mixture was heated at reflux for 30 min followed by removal of the methanol (Rotovap). The residue was taken up in 75 mL of glacial acetic acid, and diethyl oximinomalonate (17.5 g, 95 mmols) was added in one portion. Zinc dust (12.5 g) was added slowly, such that the reaction temperature was maintained between 85–95°C. After the addition was complete, the reaction mixture was heated at reflux for 1 h then decanted into 2 L of ice-water. The solid product was collected by filtration and recrystallized from methanol–water to yield 6.1 g pure product (62% yield). It had mp 73–75°C (lit.[9] mp 74–76°C); GC-MS, *m/z* (rel. intens): 209, 194, 162, 148 (100%), 120, 91, 77, 53 amu; and ^1H NMR ($CDCl_3$, 300 MHz) 1.08 (t, J=7.5 Hz, 3 H), 1.15 (t, J=7.5 Hz, 3 H), 1.35 (t, J=7.5 Hz, 3 H), 2.21 (s, 3 H), 2.39 (q, J=7.5 Hz, 2 H), 2.72 (q, J=7.5 Hz, 2 H), 4.30 (q, J=7.5 Hz, 2 H), 8.80 (s, 1 H) ppm.

3-Ethyl-2,4-Hexanedione-O^2,O^4-difluoroboronate (14). Boron trifluoride etherate (59 mL, 0.48 mol) and 2-pentanone (50 mL, 0.47 mol) were added to a 1 L round-bottom flask fitted with a drying tube (anhydr. $CaCl_2$) and equipped for magnetic stirring. The solution was stirred for 2 h at room temperature, then propionic anhydride (60 mL, 0.47 mol) was added, and the reaction mixture was heated at reflux for 2 h. The solution was then poured into 2 L of ice-water, and the solid complex was collected by filtration (vacuum). The crude product was recrystallized from methanol–water to give the desired product, 32 g, in 38% yield. It had mp 76–77°C (lit.[15] mp 75–77°C); and ^1H NMR ($CDCl_3$, 300 MHz) 1.10 (t, J=7.5 Hz, 3 H), 1.25 (t, J=7.5 Hz, 3 H), 2.34 (s, 3 H), 2.36 (q, J=7.5 Hz, 2 H), 2.63 (q, J=7.5 Hz, 2 H) ppm.

Acknowledgements

We thank the US National Institutes of Health (HD 17779) for generous support of this work. We also thank Prof. T. W. Bell of our department for generous use of the vapor pressure osmometry apparatus. Michael T. Huggins is an R. C. Fuson Graduate Fellow.

References

1. Chowdury, J. R.; Wolkoff, A. W.; Chowdury, N. R.; Arias, I. M. Hereditary Jaundice and Disorders of Bilirubin Metabolism. In *The Metabolic and Molecular Bases of Inherited Disease*, Scriver,

C. R.; Beaudet, A. L.; Sly, W. S.; Valle, D., Eds.; McGraw-Hill: New York, 1979; II, pp 2161–2208.
2. McDonagh, A. F. In *The Porphyrins*, Dolphin, D., Ed.; Academic Press: New York, 1979; 6, pp 293–491.
3. For leading references, see Falk, H. *The Chemistry of Linear Oligopyrroles and Bile Pigments*; Springer: Vienna, 1989.
4. Nogales, D. F.; Ma, J.-S.; Lightner, D. A. *Tetrahedron* **1993**, *49*, 2361–2372.
5. Person, R. V.; Peterson, B. R.; Lightner, D. A. *J. Am. Chem. Soc.* **1994**, *116*, 42–59.
6. (a) Falk, H. Molecular Structure of Bile Pigments. In *Bilirubin*; Heirwegh, K. P. M.; Brown, S. B., Eds.; CRC Press: Boca Raton, FL, 1982; Vol. 1, pp 7–29. (b) Shelver, W. L.; Rosenberg, H.; Shelver, W. H. *Intl. J. Quantum Chem.* **1992**, *44*, 141–163. (c) Shelver, W. L.; Rosenberg, H.; Shelver, W. H. *J. Mol. Struct.* **1994**, *312*, 1–9.
7. (a) Nogales, D.; Lightner, D. A. *J. Biol. Chem.* **1995**, *270*, 73–77. (b) Dörner, T.; Knipp, B.; Lightner, D. A. *Tetrahedron* **1997**, *53*, 2697–2716.
8. (a) Bonnett, R.; Davies, J. E.; Hursthouse, M. B.; Sheldrick, G. M. *Proc. R. Soc. London, Ser. B* **1978**, *202*, 249–268. (b) LeBas, G.; Allegret, A.; Mauguen, Y.; DeRango, C.; Bailly, M. *Acta Crystallogr., Sect. B* **1980**, *B36*, 3007–3011. (c) Becker, W.; Sheldrick, W. S. *Acta Crystallogr., Sect. B*, **1978**, *B34*, 1298–1304. (d) Mugnoli, A.; Manitto, P.; Monti, D. *Acta Crystallogr., Sect. C* **1983**, *38*, 1287–1291.
9. (a) Lightner, D. A. *Photochem. Photobiol.* **1977**, *26*, 427–436. (b) Lightner, D. A.; Park, Y.-T. *Tetrahedron* **1979**, *35*, 463–471. (c) Lamola, A. A.; Braslavsky, S. E.; Schaffner, K.; Lightner, D. A. *Photochem. Photobiol.* **1983**, *37*, 263–270. (d) Landen, G. L.; Park, Y.-T.; Lightner, D. A. *Tetrahedron* **1983**, *39*, 1893–1907. (e) Byun, Y. S.; Lightner, D. A. *J. Org. Chem.* **1991**, *56*, 6027–6033. (f) McDonagh, A. F.; Lightner, D. A.; Agati, G. *Montash. Chem.* **1998**, *129*, 649–660.
10. Trull, F. R.; Ma, J.-S.; Landen, G. L.; Lightner, D. A. *Israel J. Chem.* **1983**, *23*, 211–218.
11. Tipton, A. K.; Lightner, D. A. *Montash. Chem.* **1999**, *130*, 425–440.
12. Chen, Q.; Lightner, D. A. *J. Org. Chem.* **1998**, *63*, 2665–2675.
13. (a) Galliani, G.; Monti, D.; Speranza, G.; Manitto, P. *Tetrahedron Lett.* **1984**, *25*, 6037–6040. (b) Ostrow, J. D. *Semin. Hematol.* **1972**, *9*, 113–125.
14. Chen, Q. Q.; Huggins, M. T.; Lightner, D. A.; Norona, W.; McDonagh, A. F. *J. Am. Chem. Soc.* **1999**, *40*, 9253–9264.
15. Wang, C.-B.; Chang, C. K. *Synthesis* **1979**, 548–549.
16. (a) Xie, M.; Lightner, D. A. *Tetrahedron* **1993**, *49*, 2185–2200. (b) Kar, A.; Lightner, D. A. *Tetrahedron* **1998**, *54*, 12671–12690. (c) Boiadjiev, S.; Lightner, D. A. *J. Org. Chem* **1998**, *63*, 6220–6228.
17. (a) Kaplan, D.; Navon, G. *Israel J. Chem.* **1983**, *23*, 177–186. (b) Kaplan, D.; Navon, G. *Biochem. J.* **1982**, *201*, 605–613. (c) Navon, G.; Frank, S.; Kaplan, D. *J. Chem. Soc., Perkin Trans. 2* **1984**, 1145–1149.
18. (a) Boiadjiev, S. E.; Anstine, D. T.; Lightner, D. A. *J. Am. Chem. Soc.* **1995**, *117*, 8727–8736. (b) Boiadjiev, S. E.; Anstine, D. T.; Maverick, E.; Lightner, D. A. *Tetrahedron: Asymmetry* **1995**, *6*, 2253–2270.
19. Manitto, P.; Monti, D. *J. Chem. Soc. Chem. Commun.* **1976**, 122–123.
20. Molecular dynamics calculations were carried out on an SGI Octane workstation using version 6.5.1 of SYBAL (Tripos Assoc., St. Louis, MO) as described in Ref. [5]. The ball and stick drawings were created from the atomic coordinates of the molecular dynamics structures using Müller and Falk's 'Ball and Stick' program for the Macintosh.